Structures of Ternary Complexes of Rat DNA Polymerase β, a DNA Template-Primer, and ddCTP

Huguette Pelletier, Michael R. Sawaya, Amalendra Kumar, Samuel H. Wilson, Joseph Kraut

Two ternary complexes of rat DNA polymerase β (pol β), a DNA template-primer, and dideoxycytidine triphosphate (ddCTP) have been determined at 2.9 Å and 3.6 Å resolution, respectively. ddCTP is the triphosphate of dideoxycytidine (ddC), a nucleoside analog that targets the reverse transcriptase of human immunodeficiency virus (HIV) and is at present used to treat AIDS. Although crystals of the two complexes belong to different space groups, the structures are similar, suggesting that the polymerase-DNA-ddCTP interactions are not affected by crystal packing forces. In the pol β active site, the attacking 3′-OH of the elongating primer, the ddCTP phosphates, and two Mg^{2+} ions are all clustered around Asp^{190}, Asp^{192}, and Asp^{256}. Two of these residues, Asp^{190} and Asp^{256}, are present in the amino acid sequences of all polymerases so far studied and are also spatially similar in the four polymerases—the Klenow fragment of *Escherichia coli* DNA polymerase I, HIV-1 reverse transcriptase, T7 RNA polymerase, and rat DNA pol β—whose crystal structures are now known. A two-metal ion mechanism is described for the nucleotidyl transfer reaction and may apply to all polymerases. In the ternary complex structures analyzed, pol β binds to the DNA template-primer in a different manner from that recently proposed for other polymerase-DNA models.

DNA replication (*1*) is a highly complex biological process, even for a relatively simple organism such as *Escherichia coli*. During replication, the double helical DNA molecule is unwound, and the two resultant single strands of DNA act as templates to guide the synthesis, one complementary base at a time, of antiparallel primer strands. Although many auxiliary proteins such as ligases, helicases, and topoisomerases are usually involved, the chemical reaction at the core of DNA replication, the nucleotidyl transfer reaction, is catalyzed by DNA polymerases and may be depicted as follows:

$$\text{Template—primer}_n + \text{dNTP} \rightarrow$$
$$\text{template-primer-dNMP}_{n+1} + \text{PP}_i$$

where dNTP (2′-deoxyribonucleoside 5′-triphosphate) represents any one of four deoxynucleotides (dATP, dGTP, dCTP, and dTTP), and dNMP and PP_i represent 2′-deoxyribonucleoside 5′-monophosphate and pyrophosphate, respectively (Fig. 1).

Inhibition of a polymerase that effects genomic replication can be fatal to an organism. In a common type of polymerase inhibition, 2′,3′-dideoxynucleotides (ddNTPs) act as chain terminators of the primer strand. The ddNTPs differ from their cellular dNTP counterparts by the absence of an attacking 3′-hydroxyl group (3′-OH) (Fig. 2) and therefore, once a dideoxynucleotide is successfully incorporated into a growing primer strand, there can be no further incorporation of subsequent nucleotides. A well-known example of this kind of inhibition involves HIV-1 reverse transcriptase (RT), which is the polymerase responsible for the replication of the HIV genome. 3′-azido-2′,3′-dideoxythymidine (AZT), 2′,3′-dideoxyinosine (ddI), and 2′,3′-dideoxycytidine (ddC) are all anti-HIV drugs (*2*, *3*) that become potent chain termination inhibitors of RT after they are converted by cellular kinases (*4*, *5*), in vivo, to their corresponding nucleoside 5′-triphosphates, AZT-TP, ddATP (*6*), and ddCTP, respectively. In that all polymerases probably share a common catalytic mechanism, it is not surprising that some toxic effects of these drugs have been attributed to inhibition of host-cell polymerases, perhaps including the pol β described here (*7*–*9*). Therefore, a detailed understanding of the nucleotidyl transfer reaction, as well as the mechanism of inhibition of viral and host cell polymerases by nucleoside analogs, may lead to the design of more potent and less toxic HIV-1 RT inhibitors for use in the treatment of AIDS.

Despite limited sequence similarity to the Klenow fragment (KF) of *E. coli* DNA pol I [the only other polymerase for which a crystal structure (*10*) was known at the time], the crystal structure determinations of HIV-1 RT (*11*, *12*) revealed a common polymerase fold consisting of three distinct subdomains (designated fingers, palm, and thumb because of the resemblance to a hand) forming an obvious DNA binding channel. The strongest structural overlap between KF and RT comprised a trio of carboxylic acid residues located in the palm subdomain (*11*, *12*). These observations led to the hypothesis that perhaps all polymerases share a common nucleotidyl transfer mechanism centered around the highly conserved carboxylic acid residues (*11*). Strengthening this argument somewhat was the subsequent crystal structure determination of an RNA polymerase (RNAP) from bacteriophage T7, which showed strong structural similarities with KF (*13*). How-

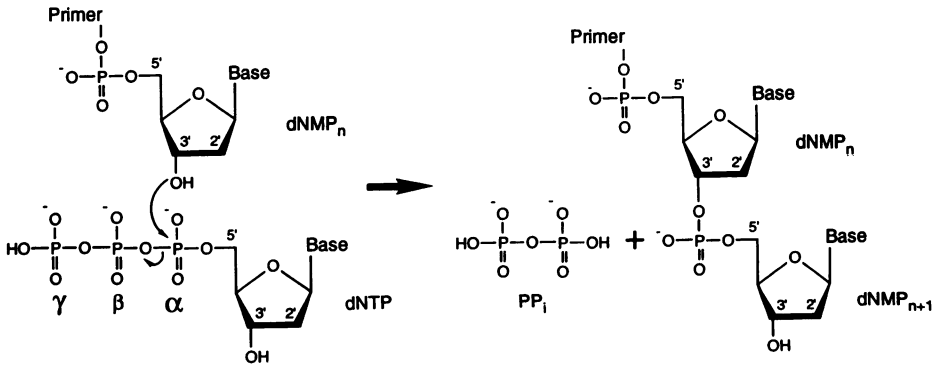

Fig. 1. The nucleotidyl transfer reaction. The 3′-OH group of the terminal dNMP on the primer strand attacks the 5′–α phosphate of an incoming dNTP, and a newly formed phosphodiester linkage results in elongation of the primer strand by one dNMP. After release of pyrophosphate (PP_i), the catalytic cycle is complete and the 3′-OH group of the newly incorporated dNMP is now ready to attack yet another incoming dNTP. Only the 3′ end of a primer is extended so that DNA polymerization is said to proceed in a 5′ to 3′ direction. If the polymerase molecule does not release the template-primer before incorporation of a second dNMP, the mode of DNA synthesis is said to

H. Pelletier, M. R. Sawaya, and J. Kraut are in the Department of Chemistry, University of California, San Diego, CA 92093–0317, USA. A. Kumar and S. H. Wilson are at the Sealy Center for Molecular Science

ever, because structural evidence for a common nucleotidyl transfer mechanism has so far been limited to comparisons among polymerases from a bacterium (KF), a virus (RT), and a phage (RNAP), perhaps the most convincing evidence for this hypothesis is provided by the crystal structure determination of a eukaryotic polymerase, rat DNA pol β (*14*). Sequence alignments show that pol β is so distantly related, even from its eukaryotic relatives, polymerases α, γ, δ, and ε, that it stands in a class of its own along with only one other polymerase, terminal deoxynucleotidyltransferase (TdT) (*15*). The crystal structure of pol β nevertheless revealed a polymerase fold consisting of palm, fingers, and thumb (along with an additional 8-kD domain attached to the fingers), and the most striking structural similarity with its distant relatives, KF, RT, and RNAP, is a portion of the palm that bears the highly conserved carboxylic acid residues (*14*). This suggests that despite the large differences in size (pol β, at 39 kD, is the smallest polymerase known), in function [although pol β may play a role in DNA replication (*16, 17*), its primary function is in DNA repair (*18–20*)], and in fidelity [pol β is the most error prone eukaryotic polymerase studied to date (*21, 22*)], pol β probably shares a common nucleotidyl transfer catalytic mechanism with all other polymerases.

Taking advantage of the chain termination method of polymerase inhibition with ddNTPs, we have succeeded in growing crystals of rat pol β complexed with two pseudo substrates, namely, (i) a DNA template-primer in which the 3′ end of the primer has been "terminated" by ddCMP, and (ii) ddCTP. In preparation for crystallization experiments, we mixed pol β with the DNA template-primer shown below and a large excess of ddCTP on the assumption that, prior to crystallization, the following reaction would occur:

$$\begin{array}{l} 3'GCCGCGGGAAA5' \\ 5'CGGCGC \quad 3' + ddCTP \rightarrow \\ \qquad 3'GCCGCGGGAAA5' \\ \qquad 5'CGGCGCC_{dd} \quad 3' + PP_i \end{array}$$

where C_{dd} is the newly incorporated ddCMP. If pol β then were to try to incorporate another nucleotide onto the primer terminus, a second nucleotidyl transfer reaction could not occur because the recently incorporated ddCMP lacks a 3′-OH group. This should result in a pseudo Michaelis-Menten ternary complex in which both "substrates" are present, namely, a nonreactive template-primer and a nucleoside triphosphate. Crystals were obtained, and the subsequent structure determinations revealed that this must have been showed a primer strand that was seven nucleotides long, although we started with a primer that was only six nucleotides in length, and the 3′ (deoxy) terminus of the primer was positioned next to strong electron density resembling a nucleoside triphosphate, presumably ddCTP.

Such a detailed view of the active site in the ternary complex allows us to propose a two-metal ion mechanism for the nucleotidyl transfer reaction that is similar, in many ways, to the two-metal ion mechanism previously proposed for another type of phosphoryl transfer reaction—the exonuclease reaction of the 3′→5′ exonuclease of *E. coli* DNA pol I (*23, 24*). Our proposed nucleotidyl transfer mechanism probably applies to all polymerases, but when we attempt to extend that mechanism to the other three polymerases—KF, RT, and RNAP—for which the crystal structures are known, a problem arises: in our structures, pol β is bound to the DNA in a manner that differs from the recently proposed polymerase-DNA models for all three of these polymerases.

Crystallizations and preliminary diffraction studies. Recombinant rat DNA pol β (*25*) was expressed in *E. coli* and purified as described (*26*). After purification, the protein was washed three times in a microconcentrator (Centricon-10, Amicon) with a buffer solution (10 mM ammonium sulfate, 0.1 M tris, pH 7.0), then concentrated to 20 mg/ml and stored at −80°C in sealed Eppendorf tubes (120-μl portions). Prior to crystallization, a protein-DNA-ddCTP sample was prepared at room temperature; approximately 1.2 mg of the 11-nucleotide (nt) template and 0.8 mg of the 6-nt primer (*27*) were dissolved in 240 μl of a buffer solution (20 mM $MgCl_2$, 0.1 M MES, pH 6.5) and the mixture was left in a sealed Eppendorf tube for 1 hour to allow annealing of the template-primer (*28*). Two portions of pol β (240-μl of a solution containing 20 mg/ml) were then thawed and added, and the protein-template-primer sample was allowed to stand for an additional hour. A 4-μmol sample of ddCTP (in 40 μl of H_2O) (*29*) was the last component to be added, resulting in a reaction mixture containing pol β at approximately 10 mg/ml, 10 mM $MgCl_2$, and an excess of template:primer:ddCTP in molar ratios of 3:4:30, respectively, relative to the amount of protein. The reaction, nucleotidyl transfer of ddCMP to the primer 3′ terminus, was allowed to proceed for 2 hours before crystallization trays were set up (*30*).

Two different crystal forms were observed, depending on the concentration of lithium sulfate in the reservoir solution. One crystal form, obtained with lithium sulfate concentrations from 40 to 75 mM, was hexagonal and grew to dimensions of 0.8 by 0.8 by 0.6 mm in about 2 weeks. These crystals belong to space group $P6_1$ ($a = b = 94.9$, $c = 117.6$ Å), with one complex molecule per asymmetric unit. Under similar conditions, but at lithium sulfate concentrations from 75 to 150 mM, platelike crystals grew to dimensions of

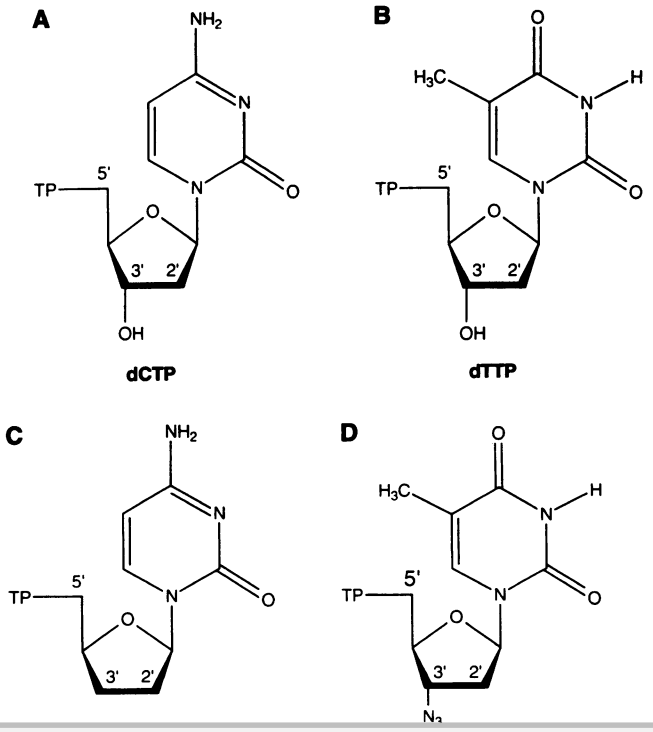

Fig. 2. Two normal cellular nucleotides, (**A**) 2′-deoxycytidine 5′-triphosphate (dCTP) and (**B**) 2′-deoxythymidine 5′-triphosphate (dTTP), and their anti-HIV (drug) counterparts (**C**) 2′,3′-dideoxycytidine 5′-triphosphate (ddCTP) and (**D**) 3′-azido-2′,3′-dideoxythymidine 5′-triphosphate (AZT-TP). The triphosphate moiety, which is linked via a phosphoester bond to the 5′ carbon of the ribose, is designated TP.

1.0 by 0.6 by 0.2 mm in a few days. These crystals belong to space group $P2_1$ (a = 106.3, b = 56.8, c = 86.7 Å, and β = 106.4°) and there are two complex molecules per asymmetric unit. Often both crystal forms grew in the same drop, and the crystals on which data were collected (Table 1) were grown at the same concentration of lithium sulfate, 75 mM. The unusually large excess of ddCTP (1:30 molar ratio) was required in order to obtain the $P6_1$ crystals, but the $P2_1$ crystals could be grown under much lower ddCTP excesses (1:10 molar ratio). Extreme purity of all components in the crystallization medium, particularly the DNA samples (*27*), seemed to be an absolute requirement for growing both types of ternary complex crystals.

Attempts were made to obtain ternary complex crystals of rat pol β, a DNA template-primer, and AZT-TP (Fig. 2D) (*31*) under similar conditions, even though incorporation of AZT-MP would result in a mismatched base pair (of a G-T type) at the primer terminus (*22*). Orthorhombic crystals grew in space group $P2_12_12$ (a = 188.4, b = 67.7, c = 39.1 Å) with one pol β molecule in the asymmetric unit. A 4.0 Å data set was collected and preliminary structural studies (*32*) showed that, because of crystal packing, it was not possible for the template-primer to occupy the pol β binding channel. Failure of pol β to form a tight complex with the DNA template-primer under these conditions might be attributed to steric hindrance by the azido group of a newly incorporated AZT-MP on the primer terminus.

Efforts to obtain a binary complex of pol β and a DNA template-primer alone (neither ddCTP nor AZT-TP) resulted in crystals that grew under much different conditions, but were nonetheless isomorphous with the $P2_12_12$ (AZT-TP) crystals mentioned above. Failure of pol β to bind to the DNA in this case could be due to the higher salt concentration of the crystallization medium (about 250 mM salt compared to 75 mM). Because one crystallization medium contained AZT-TP and the other did not, we calculated $F_{0(\text{AZT-TP})} - F_{0(\text{apo})}$, α_c, difference Fourier maps to see whether an AZT-TP binding site could be located. Strong electron density was observed in an area of the map adjacent to Arg^{149}, which is near the catalytically important residues, Asp^{190}, Asp^{192}, and Asp^{256}. This pol β–AZT-TP binary complex which, as discussed below, is probably not catalytically relevant, is similar to a KF-dNTP binary complex in which the dNTP bound to Arg residues near the catalytically important carboxylic acid residues of KF (*33*).

Human pol β, which has been cloned and expressed (*34, 35*) in a manner similar to that of rat pol β, shares more than 95 percent sequence similarity with rat pol β, so it was somewhat surprising when attempts to obtain ternary complex crystals of human pol β, a DNA template-primer, and ddCTP under the same conditions described above for the rat enzyme resulted in crystals that grew in two previously unobserved orthorhombic crystal forms. One form has unit cell parameters a = 158, b = 108, c = 60 Å, with probably two complex molecules in the asymmetric unit, but the crystals diffract only to about 5 Å resolution. In contrast, the second crystal form diffracts quite well (to about 3.3 Å), but its unit cell parameters of a = 465, b = 168, c = 56 Å are so large that special data collection techniques would be required.

Structure determination and refinement. Data collection and refinement statistics for the structure determinations of the two ternary complexes of rat pol β, a DNA template-primer, and ddCTP are listed in Table 1. Structure solutions utilized the refined atomic coordinates of the high resolution (2.3 Å) structure of the 31-kD domain of rat pol β (*14*). The molecular replacement programs of XPLOR (*36*) gave clear rotation solutions for the 31-kD domain of both ternary complexes, but only after results from classical cross-rotation searches had been filtered through the Patterson-correlation (PC) refinement steps (*37*). PC refinement techniques were particularly powerful for our structure determinations because independent rigid body movements of the fingers, palm, and thumb subdomains of the 31-kD domain could be allowed during PC refinement of the rotation searches. Results from subsequent translation searches gave solutions for the $P6_1$ complex structure that were, in general, at higher peak height to background ratios than translation solutions for the $P2_1$ complex structure, but the highest translation peaks in both cases nevertheless were the correct solutions (*38*).

The 31-kD partial structure solutions obtained by molecular replacement techniques were subjected to rigid body refinement by XPLOR (*36*), where the entire 31-kD domain was first allowed to move as a rigid body, then later, the fingers, palm, and thumb subdomains were allowed to move as independent rigid bodies simultaneously. Typical R factors at this stage were about 50 percent. After subsequent positional refinement with the least squares program package TNT (*39*) had lowered the R factors of the partial solutions to about 45 percent, we calculated $F_0 - F_c$, α_c, difference Fourier maps that revealed clear electron density for many of the backbone phosphates of a double-stranded DNA molecule as well as the three phosphates of a ddCTP nucleotide, and even portions of the 8-kD domain were evident at this early stage. Cycles of model building and least squares refinement improved the electron density for the rest of the DNA as well as the 8-kD domain for both complex structures, and once the R factors had dropped below 30 percent, refinement of individual isotropic temperature factors also improved the maps and facilitated refinement.

Although we were unable to discern the DNA base sequences at these resolutions, the directionality (5′ → 3′) of the DNA strands was evident early in our modeling efforts, hence we knew that the 3′ terminus of either the template strand or the primer strand was positioned at the pol β active

Table 1. Data collection and refinement statistics. X-ray diffraction data were collected on a multiwire area detector (*98*) (San Diego Multiwire Systems) with monochromatized CuKα radiation (Rigaku rotating anode x-ray generator), and intensity observations for each data set were processed with a local UCSD Data Collection Facility software package (*99*). Reflections from 20 Å to the maximum resolution were included in all least squares refinement steps. The final structures for both complexes include all residues, with the exception of residues 1 to 8 of the disordered NH_2-terminus and residues 246 to 248 of a disordered surface loop. There are a few missing side chain atoms in both coordinate sets that are mainly in lysine and arginine residues of the 8-kD domain. Omit maps were used to confirm the modeling of the DNA template-primer, the ddCTP nucleotide, and the cis-peptide bond between Gly^{274} and Ser^{275}.

Data collection							Refinement			
Space group	d_{min} (Å)	$\frac{I}{\sigma}$*	Reflections		Completeness (%)	R_{sym}†	Atoms‡	rms deviation§		Final R‖
			Total	Unique				Bond (Å)	Angle (°)	
$P6_1$	2.9	1.8	53,583	13,281	99	0.087	2914	0.020	2.9	0.193
$P2_1$	3.6	1.8	25,046	10,650	96	0.059	5753	0.018	2.9	0.199

*Average ratio of observed intensity to background in the highest resolution shell of reflections. †$R_{sym} = \Sigma|I_{obs} - I_{avg}|/\Sigma I_{avg}$. ‡The number of nonhydrogen atoms includes 31 and 4 water oxygens for the $P6_1$ and the $P2_1$ structures, respectively. §The rms bond and rms angle values are the deviations from ideal values of the bond

able to model in seven nucleotides for one of the DNA strands and at least 8 nt for the second DNA strand. Provided that no unexpected side reactions had occurred during crystallization, we knew that the primer could be no longer than 7 nt, and therefore the DNA strand containing 8 nt was designated the template. We then concluded that the first three bases of the template (AAA) are disordered in both crystal structures. This interpretation of the data is in agreement with the idea that the 3′ terminus of the primer should be positioned at the polymerase active site. Analysis of the DNA in our refined structures with the program CURVES II (*40*) indicated that the DNA is predominantly B form. Our DNA may have some A-DNA characteristics, however, in that the minor groove width appears to increase as the DNA approaches the pol β active site; the section of the double-stranded DNA that is removed from the active site and protrudes into solution is characteristic of B-DNA with a minor groove width of 11 Å, whereas nearer to the active site, the minor groove width is almost 15 Å (typical A-DNA has a minor groove width of about 17 Å).

Description of the structures. When the pol β ternary complex structures are compared with the structure of the apo enzyme (Fig. 3), the most apparent differences consist of large movements of the 8-kD NH_2-terminal domain relative to the fingers, palm, and thumb of 31-kD COOH-terminal domain. The 8-kD domain is tethered to a proteolytically sensitive hinge region (residues 80–90) and changes from an open conformation in the apo structure to more closed conformations in the complex structures. Because of the precarious position of the 8-kD domain in the pol β apo structure, this type of conformational change seemed inevitable even before the structures of the ternary complexes were determined. The only other significant conformational changes on complex formation were noticeable rigid-body movements of the thumb and, to a lesser degree, the fingers, resulting in a somewhat more tightly closed hand in the ternary com- plexes. A greater degree of flexibility on the part of the thumb subdomain has also been observed in other polymerase-DNA structures (*12, 23, 24, 41*). A least squares superposition of the 31-kD domain of the apo structure (*14*) on the 31-kD domain of one of the ternary complex structures ($P6_1$) resulted in a root-mean-square (rms) deviation in α carbon positions of 2.5 Å, whereas when the fingers, palm, and thumb subdomains were treated separately, the rms deviations in α carbon positions were only 0.71, 0.69, and 0.82 Å, respectively.

The 8-kD domain has a net charge of

binds to single stranded DNA with an association constant of $2 \times 10^5\ M^{-1}$ (*26*). It has no obvious structural equivalent in any of the other polymerases for which crystal structures have been determined, and crosslinking studies with gapped DNA substrates (*42*) suggest that the 8-kD domain is probably responsible for the highly

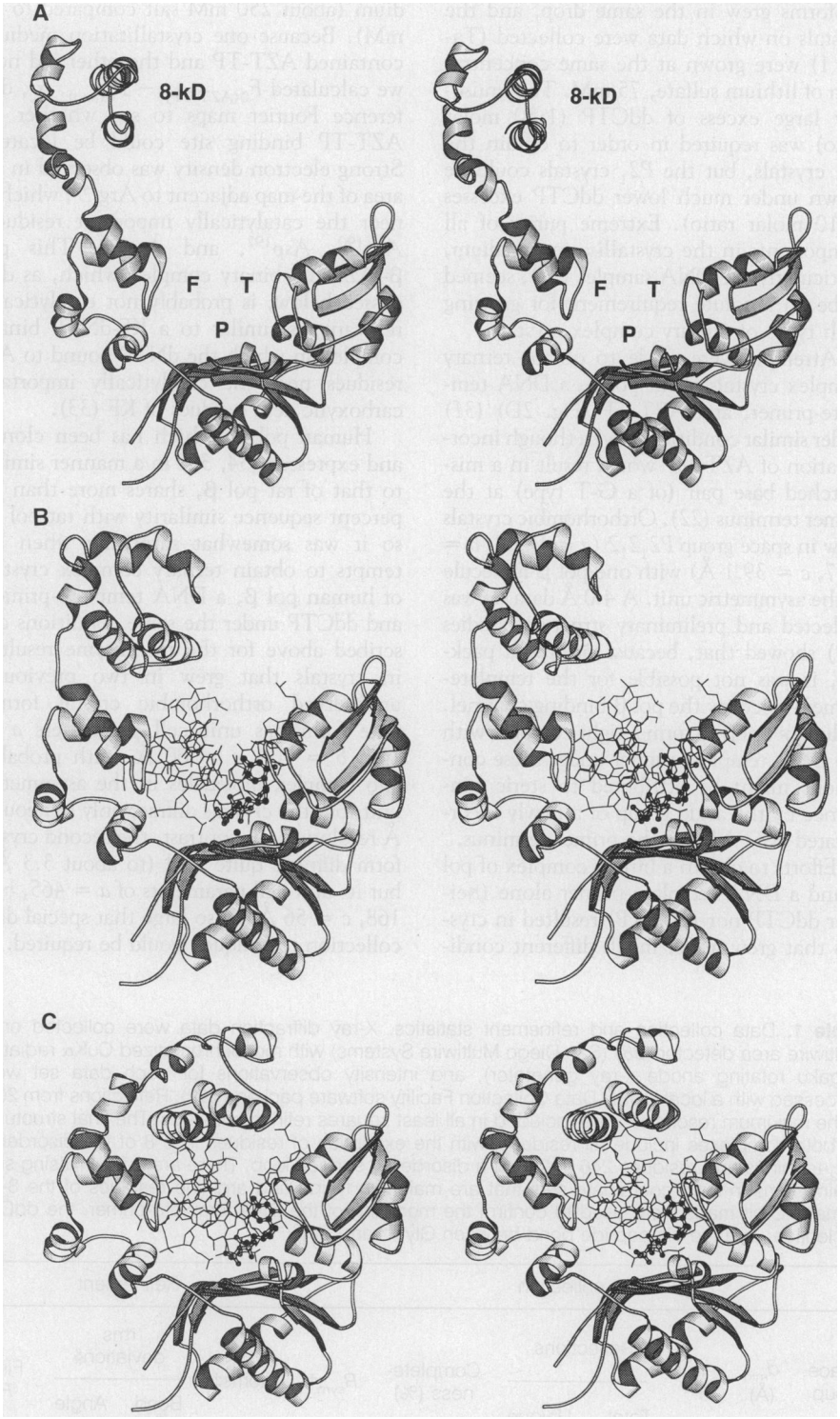

Fig. 3. Stereoview ribbon diagrams (*100*) of (**A**) rat DNA pol β, apo structure (*14*) and (**B** and **C**) ternary complexes of rat DNA pol β with a DNA template-primer and ddCTP in space groups $P6_1$ and $P2_1$, respectively. In (A) the 8-kD domain is designated 8-kD, and the fingers, palm, and thumb subdomains of the 31-kD domain are represented by F, P, and T, respectively. A ball-and-stick representation highlights the ddCTP nucleotide in (B and C). In (B) the positions of the two Mg^{2+} ions are marked with black spheres. These metals ions are not shown in (C) because we were

processive short-gap filling activities found exclusively in pol β (*43*). It has been proposed that the 31-kD domain binds to the double-stranded segment of the template-primer, and the 8-kD domain binds to the single-stranded template overhang (*44*)—or in the case of binding to a short gap in the DNA, to the 5′-phosphate of the downstream oligonucleotide (*42*). We see some evidence of this in that the 31-kD domain clearly uses its palm, fingers, and thumb to grasp the double-stranded segment of the template-primer while the 8-kD domain, although positioned quite differently in the two complex structures, is nevertheless close to where an extended template would be. Unfortunately, our template overhang was probably a little too short (only four bases—GAAA) to interact strongly with the 8-kD domain, causing the first three bases of the template to be disordered in both crystal structures. It is possible that, because the highly flexible 8-kD domain had no template on which to anchor in our crystallization experiments, its position was determined almost entirely by crystal packing forces, and probably neither of the two conformations of the 8-kD domain seen in Fig. 3, B and C, is correct for template binding in vivo. Nevertheless, kinetic studies of the 31-kD fragment alone showed that pol β can still function as a polymerase without the 8-kD domain, albeit at only about 5 percent of its normal activity (*44*).

Table 2. Hydrogen bond interactions of 3.3 Å or less between pol β and the DNA template-primer.

Residue	Subdomain	Atom	Base*	Atom	Distance (Å)
		Protein to DNA phosphate H bonds			
Gly^{105}	Fingers	N	P-6C	O2P	2.9
Gly^{107}	Fingers	N	P-5G	O2P	2.7
Ser^{109}	Fingers	N	P-5G	O1P	2.9
Ala^{110}	Fingers	N	P-5G	O2P	3.1
Arg^{254}	Fingers	NH2	P-7C	O2P	2.7
Lys^{230}	Palm	N	T-9C	O2P	3.0
Thr^{233}	Palm	N	T-8G	O2P	3.1
Lys^{234}	Palm	N	T-8G	O2P	2.7
Thr^{292}	Thumb	OG1	T-5G	O2P	2.7
Tyr^{296}	Thumb	OH	T-5C	O2P	2.6
		Protein to DNA base H bonds			
Lys^{234}	Palm	NZ	T-7C	O2	2.9
Tyr^{271}	Thumb	OH	P-7C	O2	2.7
Arg^{283}	Thumb	NH1	T-4G	N3	3.2

*DNA bases are designated T or P to distinguish template bases from primer bases, respectively. Starting from the 5′ terminus of each strand, bases are numbered 1 to 11 for the template and are numbered 1 to 7 for the primer. C and G represent cytosine and guanine, respectively, and atom designations follow Protein Data Bank nomenclature.

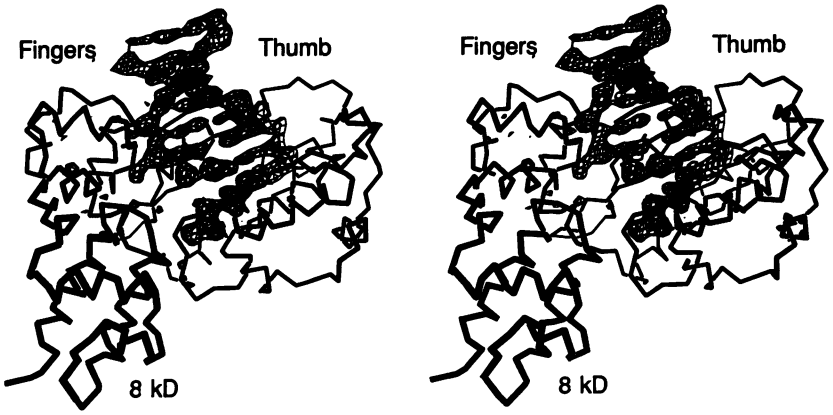

Fig. 4. Omit map of the DNA template-primer and ddCTP overlayed on an α carbon diagram of the refined *P6*$_1$ pol β structure. The view is that of Fig. 3 rotated by 90° about a horizontal axis in the plane of the page so that the DNA binding channel is now vertical. The template-primer sits on top of the palm subdomain, which is not labeled. Before all omit maps were calculated, the part of the structure in question was deleted from the coordinate file and the remaining partial structure was

In contrast to the 8-kD domain, the rest of the structure (the fingers, palm, and thumb of 31-kD domain, as well as the template-primer and ddCTP substrate) is virtually identical in both crystal forms of the ternary complex. This provides support for the physiological relevance of our complex crystals, at least with respect to the polymerase-DNA-ddCTP interactions. Also strengthening the argument is that, unlike other reported crystals of polymerase-DNA complexes (*12*, *41*), our crystals were grown at low, near physiological salt concentrations. Finally, the fact that that a ddCMP was incorporated into our template-primer shows that the nucleotidyl transfer reaction did proceed, at least for one turnover, in the same medium from which crystals were eventually obtained. In that the following discussions do not apply to the 8-kD domain of pol β and will be limited mostly to the 31-kD domain's interactions with DNA and ddCTP, we will henceforth refer only to the complex structure that has been refined to the highest resolution, the *P6*$_1$ crystal structure.

The DNA binding channel in pol β, just as in KF, RT, and RNAP, is lined with positively charged lysine and arginine side chains, and it has always been a reasonable assumption that their function is to stabilize the negatively charged backbone phosphates of the DNA (*45*). Therefore it was quite surprising that, except for Arg^{254}, which is hydrogen bonded to the phosphate of the newly incorporated ddCMP of the primer strand, there are no direct lysine or arginine interactions with the backbone phosphates of the DNA in our complex (Table 2). Instead, nearly all of the interactions of protein with DNA involve two different clusters of protein backbone nitrogens located at the entrance to the DNA binding channel (Table 2). One cluster, consisting of four of the backbone nitrogens between Gly^{105} and Ala^{110}, is located at the NH_2-terminal end of helix G in the fingers subdomain of pol β and interacts with the phosphates of the primer strand. The second cluster, comprising three of the five backbone nitrogens between Lys^{230} and Lys^{234}, is located in a beta turn, which connects beta strands 3 and 4 of the palm subdomain and interacts with backbone phosphates of the template strand. The only other hydrogen bonded interactions (3.3 Å or less) between pol β and DNA phosphates are between the side chains of Thr^{292} and Tyr^{296}, located on a loop between beta strands 6 and 7 of the thumb subdomain, and the backbone phosphates of the template strand (Table 2).

In addition to our observations that there seemed to be fewer hydrogen bond

DOCKET ALARM

Explore Litigation Insights

Docket Alarm provides insights to develop a more informed litigation strategy and the peace of mind of knowing you're on top of things.

Real-Time Litigation Alerts

Keep your litigation team up-to-date with **real-time alerts** and advanced team management tools built for the enterprise, all while greatly reducing PACER spend.

Our comprehensive service means we can handle Federal, State, and Administrative courts across the country.

Advanced Docket Research

With over 230 million records, Docket Alarm's cloud-native docket research platform finds what other services can't. Coverage includes Federal, State, plus PTAB, TTAB, ITC and NLRB decisions, all in one place.

Identify arguments that have been successful in the past with full text, pinpoint searching. Link to case law cited within any court document via Fastcase.

Analytics At Your Fingertips

Learn what happened the last time a particular judge, opposing counsel or company faced cases similar to yours.

Advanced out-of-the-box PTAB and TTAB analytics are always at your fingertips.

API

Docket Alarm offers a powerful API (application programming interface) to developers that want to integrate case filings into their apps.

LAW FIRMS
Build custom dashboards for your attorneys and clients with live data direct from the court.

Automate many repetitive legal tasks like conflict checks, document management, and marketing.

FINANCIAL INSTITUTIONS
Litigation and bankruptcy checks for companies and debtors.

E-DISCOVERY AND LEGAL VENDORS
Sync your system to PACER to automate legal marketing.